Ab initio wave function-based methods for excited states in solids: Correlation corrections to the band structure of ionic oxides

L. Hozoi, U. Birkenheuer,* and P. Fulde

Max-Planck-Institut für Physik komplexer Systeme, Nöthnitzer Strasse 38, 01187 Dresden, Germany

A. Mitrushchenkov and H. Stoll

Universität Stuttgart, Pfaffenwaldring 57, 70550 Stuttgart, Germany

Ab initio wave function-based methods are applied to the study of electron correlation effects on the band structure of oxide systems. We choose MgO as a prototype closed-shell ionic oxide. Our analysis is based on a local Hamiltonian approach and performed on finite fragments cut from the infinite solid. Localized Wannier functions and embedding potentials are obtained from prior periodic Hartree-Fock (HF) calculations. We investigate the role of various electron correlation effects in reducing the HF band gap and modifying the bandwidths. On-site and nearest-neighbor charge relaxation as well as long-range polarization effects are calculated. Whereas correlation effects are essential for computing accurate band gaps, we found that they produce smaller changes on the HF bandwidths, at least for this material. Surprisingly, a broadening effect is obtained for the O $2p$ valence bands. The *ab initio* data are in good agreement with the energy gap and bandwidth derived from thermoreflectance and x-ray photoemission experiments. The results show that the wave function-based approach applied here allows for well controlled approximations and a transparent identification of the microscopic processes which determine the electronic band structure.

I. INTRODUCTION

The proper treatment of electron correlation effects in molecules and solids stands at the heart of modern electronic structure theory.[1–5] In the study of molecular systems at least, wave function-based quantum chemistry is known to provide a rigorous theoretical framework for addressing the electron correlation problem. The standard quantum chemical methods[4,5] make possible the construction of approximate wave functions at levels of increasing sophistication and accuracy and offer thus a systematic route to converged results. Advanced wave function-based calculations can be routinely performed nowadays for small and medium size molecules. However, algorithms able to treat electron correlation effects in periodic systems are still at their infancy. The simplest correlation method is based on the Møller-Plesset equations, and second-order Møller-Plesset (MP2) perturbational schemes for solids were actually implemented by several groups.[6–14] As an extension of MP2, *ab initio* many-body Green's function techniques were developed too,[15–19] which can also be regarded as enhanced versions of the resolvent and transfer matrix methods devised already some decades ago to treat various kinds of impurities in periodic (and semi-infinite) systems on the single-particle level (e.g., Refs. 20 and 21). In addition, investigations based on coupled-cluster theory were initiated.[13,22–25]

The main point when applying quantum chemical methods to correlation calculations is to make use of the local character of the correlation hole which is surrounding an electron. The latter optimizes the Coulomb repulsion between electrons and its accurate description is the essence of the correlation treatment. Starting point is a Hartree-Fock (HF) calculation on top of which the correlation calculations are implemented. For insulators and semiconductors, the de-

velopment of efficient computational tools is facilitated by the use of optimally localized Wannier functions. Several orbital localization procedures were proposed in the context of periodic HF calculations. They normally rest on the *a posteriori* transformation of the crystal Bloch orbitals (see, for example, Refs. 6, 14, 22–24, 26, and 27). Alternative approaches were elaborated by Shukla *et al.*[28–31] and in the Toulouse group,[11,32] where the self-consistent-field (SCF) equations are solved directly in the Wannier representation.

Local correlation methods such as the incremental scheme of Stoll[33,34] and the local Hamiltonian formalism of Horsch *et al.*[35] and Gräfenstein and co-workers[36–38] were applied before to the rigorous determination of both ground-state[13,28–30] and excited-state[18,39–42] properties of infinite systems. Materials under investigation were crystalline LiH, LiF, and LiCl,[18,28–30] diamond,[40,42] silicon,[40] beryllium,[41] carbon and boron-nitrogen chains,[13] and *trans*-polyacetylene.[39] In the present work, we extend these studies to the case of ionic oxide compounds and choose MgO as a prototype and, at the same time, relatively simple insulating oxide. We compute correlation induced corrections to the valence and conduction HF energy bands and find that our final estimate for the fundamental gap is in rather good agreement with the experimental data. Our analysis also provides a clear picture of the major correlation effects that are responsible for the reduction of the HF band gap. The present study on MgO should open the way to similar calculations for more complex materials such as the $3d$ transition-metal oxides.

II. COMPUTATIONAL APPROACH

Periodic HF calculations were carried out for crystalline MgO with the CRYSTAL package.[43] Wannier functions asso-

ciated with the HF valence and low-lying conduction bands were determined with the Wannier-Boys localization module[26] of the same program. For conduction-band states, this may be a somewhat tedious task. However, localized Wannier orbitals can also be derived in more difficult cases with band disentanglement techniques.[27]

For computing the correlation induced corrections to the valence and conduction bands, we adopt the same quasiparticle picture and local Hamiltonian formalism as employed in Refs. 35–42. The physical reasoning is as follows. When an electron (or hole) is added to the N-particle system, its surroundings relax and polarize due to the additional charge. This response of the system lowers the energy it takes to add the extra electron (or hole). The particle plus the modified surroundings move together through the system in the form of a Bloch wave and define a quasiparticle. At the same time, some of the correlation contributions which are present in the ground state of the N-particle system are no longer operative in the $(N+1)$ [or $(N-1)$] -particle system because some excitations are now blocked. This effect is called loss of ground-state correlation and must be accounted for too.[35,40] A basic feature of our approach is that the correlation treatment is performed on a finite cluster $\mathcal{C}$ cut from the extended periodic system. With the cluster-in-solid embedding technique elaborated by Birkenheuer *et al.*,[40,44,45] the cluster $\mathcal{C}$ is divided into an active region $\mathcal{C}_A$ that supports the local occupied and virtual orbitals entering the post-HF calculations and a spatial "buffer" domain $\mathcal{C}_B$ including a number of atomic sites (and basis functions) whose role is to provide a good representation for the tails of the Wannier-like orbitals of the active region $\mathcal{C}_A$. Thus, $\mathcal{C} = \mathcal{C}_A + \mathcal{C}_B$. All Wannier orbitals centered in $\mathcal{C}_B$ (and also the environment) will be held frozen in the correlation calculations.

The orbital set associated with the finite-size cluster is obtained from the data supplied by the Wannier-Boys localization module of CRYSTAL.[26] The interface program[46] written for this purpose yields in addition an embedding potential corresponding to the frozen environment, i.e., the surrounding HF electron sea. The detailed procedure for constructing the embedded cluster and the associated orbital set is described elsewhere.[44,45] Here, we merely give an outline of this. The core, valence, and low-lying conduction-band cluster orbitals are generated by projecting the crystal Wannier functions onto the set of atomic basis functions attached to the cluster region $\mathcal{C}$,

$$|w_n'(\mathbf{R})\rangle = \sum_{\beta,\alpha \in \mathcal{C}} |\beta\rangle S_{\beta\alpha}^{-1} \langle\alpha|w_n(\mathbf{R})\rangle, \qquad (1)$$

where α and β are Gaussian basis functions centered within the region $\mathcal{C}$, $S_{\beta\alpha}^{-1}$ represents the inverse overlap matrix for the basis set attached to $\mathcal{C}$, $|w_n(\mathbf{R})\rangle$ is a Wannier orbital with index n and centered in the unit cell corresponding to the lattice vector $\mathbf{R}$, and $|w_n'(\mathbf{R})\rangle$ is its projected counterpart expressed exclusively in terms of basis functions centered in $\mathcal{C}$. The $|w_n'(\mathbf{R})\rangle$ functions are neither normalized nor orthogonal to each other because of the projection procedure mentioned above. Therefore, they are groupwise orthonormalized in the following order: active core, active occupied, active low-

lying conduction-band orbitals, buffer core, buffer occupied, and buffer low-lying conduction-band orbitals. This way, the contamination of the most important types of orbitals is minimized. Groupwise orthonormalization actually means the use of the Schmidt orthogonalization for the intergroup orthogonalization and the Löwdin orthonormalization inside the groups. This set of orthonormal orbitals will be denoted by $|\tilde{w}_n'(\mathbf{R})\rangle$. For the construction of the variational space to be used in the subsequent correlation calculations, we follow the prescription suggested by Pulay and Saebø.[47] So-called virtual projected atomic orbitals (PAO's) are generated from the Gaussian basis functions associated with the *active* region $\mathcal{C}_A$ by projecting out the occupied and the low-lying conduction-band orbitals $|\tilde{w}_n'(\mathbf{R})\rangle$ via a Schmidt orthogonalization scheme. Thereafter, the PAO's are Löwdin orthonormalized among themselves to facilitate their subsequent use in the correlation calculations.

By making the buffer region $\mathcal{C}_B$ sufficiently large, the original Wannier orbitals of $\mathcal{C}_A$ are well represented. For example, for the Wannier orbitals corresponding to the lowest four conduction bands of MgO and centered at a Mg site, the six ligands surrounding the given Mg ion should be included in $\mathcal{C}_A$ because large contributions arise not only from the Mg $3s$ and $3p$ basis functions but also from the nearest-neighbor (NN) oxygen $2s, 3s$ and $2p, 3p$ components. Farther neighbors need not be included in the central region $\mathcal{C}_A$ but may be put into the buffer zone $\mathcal{C}_B$ because the weight of the longer-range tails is small. Whereas a high-quality description can be easily achieved for the Wannier orbitals centered in the active region, the representation of the Wannier functions in the buffer zone is less accurate. The impact of this deficiency on the correlation calculations, however, is completely compensated by an appropriate choice of the embedding potential. Actually, the Gaussian orbital representation $V_{\alpha\beta}^{\text{emb}}$ of the embedding potential is constructed by

$$V_{\alpha\beta}^{\text{emb}} = F_{\alpha\beta}^{\text{crys}} - F[P^{\mathcal{C}}]_{\alpha\beta}, \quad \alpha,\beta \in \mathcal{C}, \qquad (2)$$

where F^{crys} is the self-consistent Fock operator from the periodic HF calculation and $F[P^{\mathcal{C}}]$ is the Fock operator associated with the density operator

$$P^{\mathcal{C}} = 2\sum_{\nu}^{\text{occ}} |\tilde{w}_\nu'\rangle\langle\tilde{w}_\nu'| \qquad (3)$$

arising from all occupied orbitals $|\tilde{w}_\nu'\rangle$ which enter the subsequent correlation calculations explicitly. This way, the correlation calculations are effectively performed in an *infinite* frozen HF environment.

The data concerning the occupied and virtual orbitals of the cluster are transferred via the CRYSTAL-MOLPRO interface[46] to the quantum chemistry program MOLPRO.[48] The same holds for the matrix representation $F_{\alpha\beta}^{\text{crys}}$ of the self-consistent Fock operator of the periodic host system. The embedding potential itself is constructed according to Eqs. (2) and (3) using the MATROP module of the MOLPRO program package.

Local electron removal and electron addition one-particle configurations can be defined in terms of the set of occupied and virtual orbitals centered within the spatial domain $\mathcal{C}_A$:

$$|\Phi_{\mathbf{R}p\sigma}^{N-1}\rangle = c_{\mathbf{R}p\sigma}|\Phi\rangle \text{ and } |\Phi_{\mathbf{R}q\sigma}^{N+1}\rangle = c_{\mathbf{R}q\sigma}^{\dagger}|\Phi\rangle, \tag{4}$$

where $c_{\mathbf{R}p\sigma}$ and $c_{\mathbf{R}q\sigma}^{\dagger}$ are annihilation and creation operators for the valence- and conduction-band σ-spin orbitals $|\widetilde{w}_p'(\mathbf{R})\rangle$ and $|\widetilde{w}_q'(\mathbf{R})\rangle$, respectively, and $|\Phi\rangle$ is the single-determinant ground-state wave function of the N-electron system. For clusters which are large enough, the Hartree-Fock valence and conduction energy bands of the periodic crystal can be recovered by diagonalizing $\mathbf{k}$-dependent matrices of the following form:

$$H_{nn'}^{\mathrm{HF}}(\mathbf{k}) = \sum_{\mathbf{R}} e^{i\mathbf{kR}}\langle\Phi_{\mathbf{0}n\sigma}^{N\mp1}|H - E_0^{\mathrm{HF}}|\Phi_{\mathbf{R}n'\sigma}^{N\mp1}\rangle. \tag{5}$$

Here, $\mathbf{0}$ stands for the reference unit cell and E_0^{HF} denotes the ground-state HF energy of the neutral N-electron system. The diagonal terms $\mathbf{R}=\mathbf{0}$, $n'=n$ in this expression are directly related to the on-site excitation energies within the Koopmans approximation,[4,5] i.e., ionization potentials

$$\mathrm{IP}_{pp}^{\mathrm{HF}}(\mathbf{0}) = \langle\Phi_{\mathbf{0}p\sigma}^{N-1}|H|\Phi_{\mathbf{0}p\sigma}^{N-1}\rangle - E_0^{\mathrm{HF}} = -\epsilon_{\mathbf{0}p}^{\mathrm{HF}} > 0 \tag{6}$$

and electron affinities

$$\mathrm{EA}_{qq}^{\mathrm{HF}}(\mathbf{0}) = E_0^{\mathrm{HF}} - \langle\Phi_{\mathbf{0}q\sigma}^{N+1}|H|\Phi_{\mathbf{0}q\sigma}^{N+1}\rangle = -\epsilon_{\mathbf{0}q}^{\mathrm{HF}}, \tag{7}$$

with the latter being negative in the case of MgO. The off-diagonal terms are the hopping matrix elements in a tight-binding representation,

$$t_{nn'}^{\mathrm{HF}}(\mathbf{R}) = \langle\Phi_{\mathbf{0}n\sigma}^{N\mp1}|H - E_0^{\mathrm{HF}}|\Phi_{\mathbf{R}n'\sigma}^{N\mp1}\rangle. \tag{8}$$

Starting from the Hartree-Fock energy bands, we include next the effects of electron correlations. Within the quasiparticle approximation, we may introduce for the $(N+1)$-particle system a wave function of the following form:

$$|\Psi_{\mathbf{R}q\sigma}^{N+1}\rangle = \exp(S)c_{\mathbf{R}q\sigma}^{\dagger}|\Psi\rangle, \tag{9}$$

where $|\Psi\rangle$ is the correlated ground-state wave function of the N-electron system. The operator S does not commute with $c_{\mathbf{R}q\sigma}^{\dagger}$ and describes the correlation hole. For a more detailed discussion, we refer to Ref. 1. Alternatively, we may write $|\Psi_{\mathbf{R}q\sigma}^{N+1}\rangle = \Omega c_{\mathbf{R}q\sigma}^{\dagger}|\Phi\rangle$, where $|\Phi\rangle$ is the SCF ground state and Ω acts like a wave or Moeller operator.[3] Therefore, when correlations are taken into account, the analog of Eq. (5) becomes

$$H_{nn'}(\mathbf{k}) = \sum_{\mathbf{R}} e^{i\mathbf{kR}}\langle\Psi_{\mathbf{0}n\sigma}^{N\mp1}|H - E_0|\Psi_{\mathbf{R}n'\sigma}^{N\mp1}\rangle, \tag{10}$$

where E_0 is the energy of the N-particle correlated ground state $|\Psi\rangle$ (see also Refs. 36–40).

The correlation hole around an added electron (or hole) consists of a short-range and a long-range part. The short-range part originates from intra-atomic and short-range inter-atomic relaxation and polarization effects. We construct the short-range part of the correlation hole by separate orbital optimizations. Thereby, the Wannier orbital to which the extra electron (hole) is attached is kept frozen and the changes within a finite region around it are determined by performing an additional SCF calculation.[40,41] This is sufficient if electron correlations are weak or moderate. If they are strong, the

response of the surroundings to the extra electron (hole) differs from the SCF HF response. The long-range part of the correlation hole consists of long-range polarization of the environment. The effect of long-range polarization on the diagonal Hamiltonian matrix elements is estimated in this paper by applying the approximation of a dielectric continuum. With the known dielectric constant of MgO, $\epsilon_0 = 9.7$, we can directly determine the polarization energy of a charge $\pm e$ outside a sphere of radius R. In addition, differential correlation effects related to the existence of a different number of electrons in the system's ground state and in the $(N\pm1)$ excited states are investigated by subsequent configuration-interaction (CI) calculations.

III. CORRELATION CORRECTIONS TO THE BAND STRUCTURE OF MgO

Magnesium oxide is a prototype closed-shell ionic material that crystallizes under normal conditions in the rocksalt structure. It is extensively used in materials science as substrate for the epitaxial growth of films of other compounds. In recent years, it has attracted renewed interest because of its use as tunnel barrier in magnetic tunnel junctions.[49] A different area where MgO attracted attention is optoelectronics. It turns out that when alloyed with ZnO, depending on the precise chemical composition, the band gap of the system can be tuned along an interval ranging from 3.3 to 7.8 eV.[50] The latter number represents the fundamental gap of MgO.[51]

The valence bands of MgO have oxygen $2p$ character, whereas the lowest conduction bands are mainly related to the Mg $3s$ and $3p$ levels, with some admixture from the O $2s,3s$ and $2p,3p$ functions. The Hartree-Fock energy bands are shown in Fig. 1. We employed for our calculations the lattice constant reported by Sasaki *et al.*, $a=4.217$ Å,[52] and Gaussian-type basis sets from the standard CRYSTAL library. Basis sets of triple-zeta quality, Mg 8-511,[53] were used for the cations and triple-zeta basis sets supplemented with polarization functions, O 8-411*,[53] were applied for the more polarizable O ions. At the Hartree-Fock level and with this choice of the basis functions, the fundamental gap of the system is 16.20 eV, i.e., 8.4 eV larger than the experimental value. As illustrated in Fig. 1, there is a separation of about 16 eV between the O $2s$ and O $2p$ bands. There is also a clear separation between the low-lying Mg $3s/3p$ complex and the other conduction bands. Density-functional calculations within the local density approximation and using the same Gaussian basis sets as for the HF calculations yield a gap of 5.0 eV between the valence and conduction bands, nearly 3 eV lower than observed in experiment.

Projected Wannier orbitals associated with the Mg $3s$, $3p$ conduction-band complex are plotted in Figs. 2 and 3. We note that the Wannier-Boys localization module of the CRYSTAL program yields a set of Mg sp^3 hybrids for the lowest four conduction-band states. In order to arrive at a set of s and (x, y, z)-like functions, we applied to those projected hybrids a Pipek-Mezey localization procedure,[54] as implemented in the MOLPRO package.[48] In this localization
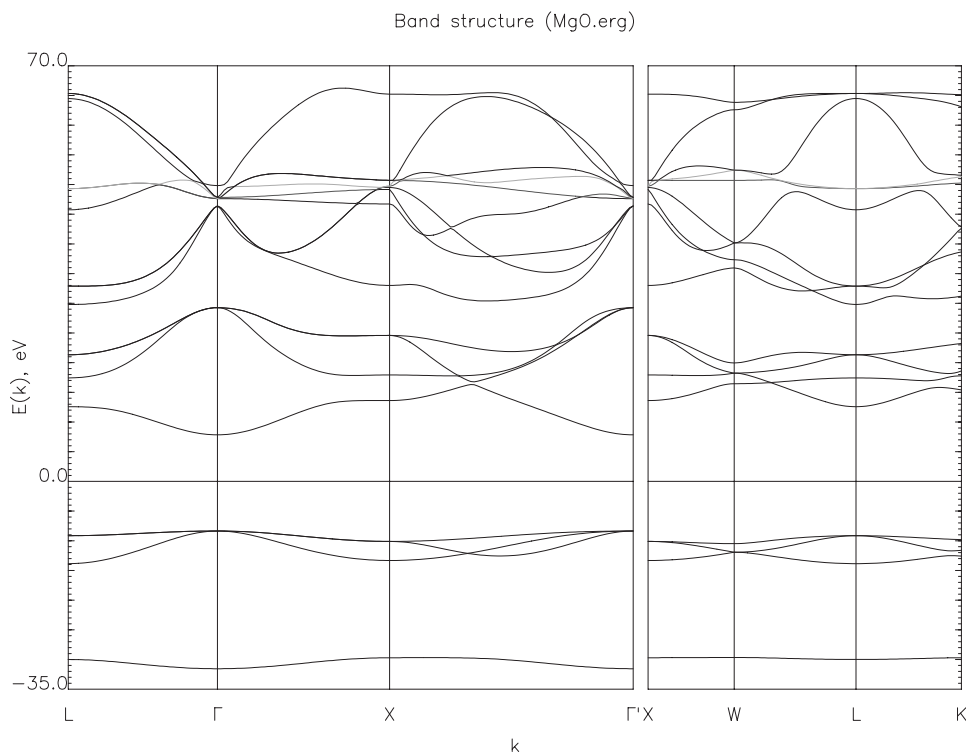
FIG. 1. Hartree-Fock band structure of bulk MgO. The core O $1s$ and Mg $1s$-$2p$ bands are not shown in the figure.

scheme, the number of atomic orbitals contributing to a given molecular-like composite is minimized. Whereas the Mg $3s$ and $3p$ Wannier functions have substantial weight at the NN ligand sites, the valence-band O $2p$ (and $2s$) Wannier orbitals are much more compact and contributions from neighboring ions are not visible in plots like those shown in Figs. 2 and 3. In the calculations reported here, the norm of the projected active orbitals is typically larger than 99.0% and never below 98.5% of the original crystal Wannier functions.

A. Correlation induced corrections to the diagonal matrix elements

Relaxation and polarization effects in the immediate neighborhood of an oxygen hole were computed by separate restricted open-shell HF (ROHF) calculations on $[O_{39}Mg_{30}]$ clusters. The multiconfiguration MCSCF module of the MOLPRO package was employed for this purpose. The active region $\mathcal{C}_A$ of the $[O_{39}Mg_{30}]$ cluster contains a central $2p^5$ (or $2s^1$) O^- ion and four of the 12 nearest O^{2-} ligands. These four oxygen neighbors are all chosen to be in the same plane and we denote them as $O_{xy}^1, \dots, O_{xy}^4$ (see Fig. 4). In addition,
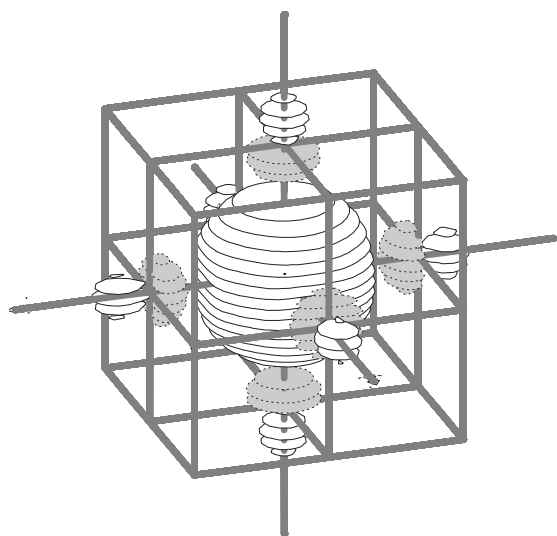

FIG. 2. Plot of the Mg $3s$-like conduction-band Wannier orbital after projection onto a $[Mg_{19}O_{14}]$ cluster. There is substantial weight at the NN oxygen sites.
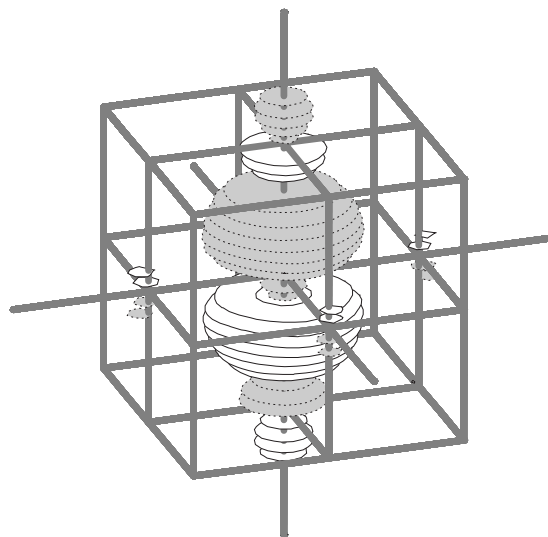

FIG. 3. Mg p-like conduction-band Wannier orbital after projection onto a $[Mg_{19}O_{14}]$ cluster.
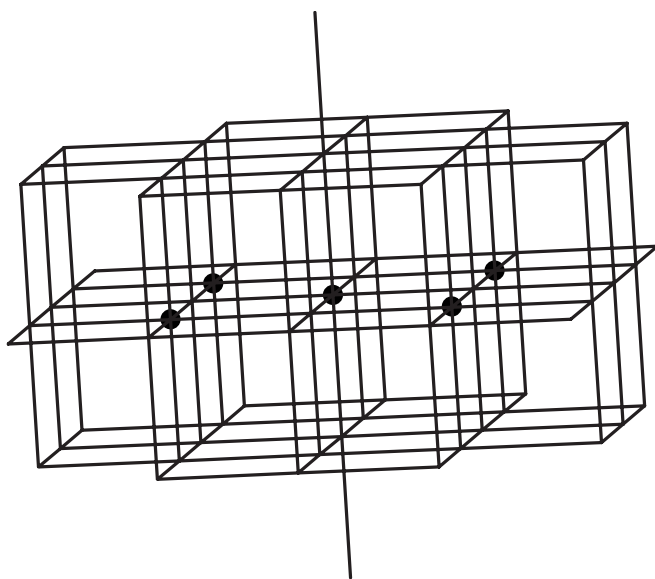
FIG. 4. Sketch of the $[O_{39}Mg_{30}]$ cluster employed for the calculation of short-range relaxation effects on the O valence-band states. The shortest line segments are Mg-O "bonds." The so-called active region $\mathcal{C}_A$ includes a central O ion and four nearest oxygen neighbors O_{xy}^i in the "horizontal" plane (see text). These active ions are shown as small black spheres.

we include in the cluster $\mathcal{C}$ the NN cations and all the O's in the next coordination shell of each of the O_{xy}^i sites, as sketched in Fig. 4. These additional Mg and O neighbors represent the so-called buffer region $\mathcal{C}_B$ and ensure an accurate description of the tails of the orbitals centered in the active region $\mathcal{C}_A$.

When performing the ROHF calculations, the oxygen hole orbital is kept frozen.[41] We also freeze in our calculations the corelike 1s, 2s, and 2p shells of all Mg ions. Orbital relaxation effects are listed in Table I for both 2s and 2p oxygen holes. The on-site relaxation effect is quite large, more than 2 eV. There is also a substantial relaxation and polarization effect associated with the first oxygen neighbors. For the four O_{xy}^i ligands included in the active region $\mathcal{C}_A$ of the cluster, this effect amounts to about 0.41 eV in the presence of an O 2s hole and to 0.40 eV in the presence of a 2p hole. In Table I, we multiplied these numbers by 3 because

TABLE I. Correlation induced corrections to the diagonal Hamiltonian matrix elements for the valence-band O 2s, 2p and conduction-band Mg 3s, 3p states. All numbers are in eV. Negative corrections induce upward shifts of the valence bands and shifts to lower energies for the conduction bands.

	$\Delta H_{nn}(\mathbf{0})$			
	O 2s	O 2p	Mg 3s	Mg 3p
On-site orb. relaxation	−2.64	−2.04		
NN orb. relaxation	−1.23	−1.20	−0.81	−0.84
Long-range polarization	−1.80	−1.80	−2.25	−2.25
Total	−5.67	−5.04	−3.06	−3.09

there is a total of 12 oxygens in that coordination shell. We obtain thus a good estimate for the relaxation and polarization effects up to the nearest O neighbors. The fact that these relaxation and polarization effects are additive was checked by extra calculations with smaller, double-zeta basis sets[53] on two different clusters: a $[O_{39}Mg_{30}]$ cluster including only the four O_{xy}^i sites in the active region and a $[O_{55}Mg_{38}]$ cluster where all 12 first oxygen neighbors were allowed to polarize.

The four lowest-energy $(N+1)$ conduction-band states imply Mg $3s^1$ or $3p^1$ electron configurations. ROHF calculations were performed for such configurations on a $[Mg_{19}O_{38}]$ cluster with a $[MgO_6]$ kernel as active region, $\mathcal{C}_A$. Beyond the $[MgO_6]$ kernel, this cluster incorporates again all Mg and O ions in the first two coordination shells of the active ligands. The on-site relaxation effects associated with the addition of an electron in a localized Mg 3s or 3p Wannier orbital are vanishingly small. The relaxation effects at the adjacent O sites induce energy shifts of 0.80–0.85 eV (see Table I). In these calculations, the open-shell active orbitals (Mg $3s^1$ or $3p^1$) were again kept frozen.[41] We note that the energetic effect is nearly the same for the $3s^1$ and $3p^1$ conduction-band states. At the scale of Fig. 1 at least, it induces a uniform downward shift of the center of gravity of the 3s-3p band complex.

The data listed in Table I indicate that the on-site orbital relaxation and relaxation and polarization effects at the nearest oxygen sites in the presence of an extra electron or extra electron hole result in a reduction of the HF band gap by about 4.05 eV, that is, more than 45% of the difference between the HF and experimental values. Large corrections are also expected to arise from long-range polarization effects. The long-range polarization energy of a dielectric due to the presence of an extra charge $\pm e$ can be expressed as[1]

$$\Delta E(\infty) = \Delta E(R) - C/R, \quad C = \frac{\epsilon_0 - 1}{2\epsilon_0}e^2, \qquad (11)$$

where ϵ_0 is the static dielectric constant of the material and R defines a sphere around the extra charge beyond which the dielectric response reaches its asymptotic value ϵ_0. The energy increment $\Delta E(R)$ denotes the relaxation and polarization energy up to the radius R around the added particle. The constant C can be obtained by choosing two different radii R_1 and R_2 where the quantities $\Delta E(R_1)$ and $\Delta E(R_2)$ are computed (see, for example, Refs. 35 and 37). However, we adopt here a simpler approach. We calculate the corrections due to long-range polarization by using the experimental value for the static dielectric constant, $\epsilon_0 = 9.7$. Since relaxation and polarization effects related to the nearest oxygen neighbors were already accounted for, both for the valence-band hole states and the conduction-band electrons (see Table I) and since the corelike electrons of the Mg^{2+} ions can be ignored in these calculations, we set R as the average of the radii of the first and second oxygen coordination shells around a localized 2p(2s) hole or 3s/3p electron: $R = (a\sqrt{2}/2 + a)/2$ for the O 2p valence-band states, where $a = 4.217$ Å is the lattice constant,[52] and $R = (a/2 + a\sqrt{3}/2)/2$ for the conduction-band states. The corrections to the diagonal matrix elements of the Hamiltonian are then

$$\Delta H_{nn}(\mathbf{0}) = -\frac{\epsilon_0 - 1}{2\epsilon_0}\frac{e^2}{R}, \qquad (12)$$

about -1.80 eV for the O $2s/2p$ bands and -2.25 eV for the Mg $3s/3p$ bands. These numbers are also included in Table I.

The validity of the continuum dielectric model in estimating the long-range polarization corrections can be checked by SCF calculations of the polarization effects at farther O sites. Around a given oxygen ion, for example, there are 12 O sites in the first O coordination shell, 6 sites in the second O coordination shell, and 24 sites in the shell of third-order O neighbors. Starting from the cluster shown in Fig. 4, we added to the active region $\mathcal{C}_A$ a second-order O neighbor of the "central" O$^-$ anion. The buffer region $\mathcal{C}_B$ of the finite fragment was also enlarged, such that it includes all Mg and O NN's of the O ion added to the active part. The SCF calculations for the valence-band $(N-1)$ states show that the polarization of this second-order O neighbor leads to corrections of 0.03 eV to the O $2s$ and O $2p$ ionization potentials. The contribution due to all six second-order O neighbors is thus about 0.18 eV. Within the approximation of a dielectric continuum, the second shell of O neighbors is responsible for a correction $\delta E_2 = S_2 C(1/R_i - 1/R_o)$ to the diagonal matrix elements of the Hamiltonian, where $R_i = (a\sqrt{2}/2 + a)/2$, $R_o = (a + a\sqrt{6}/2)/2$, and $S_2 = 0.47$ is a scaling factor which describes the fact that the number (or density) of O sites in the shell enclosed between the radii R_i and R_o is smaller than the number of ligands in the unit cell. We find then a value of 0.19 eV for δE_2, which compares very well with the result of the *ab initio* calculation, 0.18 eV. The scaling factor S_i shows an oscillatory behavior for consecutive shells. For the shell of third-order oxygen neighbors, $S_3 = 1.56$. For infinitely large R, however, it holds that $S \rightarrow 1$. The above show that Eq. (11) is sufficiently accurate in describing the long-range polarization cloud around an additional charge in the solid.

Before we discuss band narrowing (or broadening) due to correlation effects which also affect the band gap, we consider the loss of ground-state correlations. The latter leads again to a shift of the center of gravity of the bands. As pointed out in the previous section, some of the configurations that are present in the N-particle ground-state are blocked when an electron is added or removed. We investigated such correlations by CI calculations with single and double excitations (CISD) and discuss first differential effects for the N and $(N-1)$ states. Since the oxygen valence-band Wannier orbitals are rather localized, we designed a cluster with a single O ion in the active region. Around this central O site, we added one shell of Mg ions (6 Mg's) and two shells of anions (12+6 O's) to build the buffer region $\mathcal{C}_B$. In the CISD calculations for the N and $(N-1)$ configurations, we correlate the $2s$ and $2p$ orbitals of the central O ion. Thereby, the occupancy of the hole orbital is kept frozen in the calculations for the $(N-1)$ states, which is referred to as the frozen hole approximation.[40,41] Sets of separately optimized orbitals were used for the hole states of the $(N-1)$-particle system, as discussed above. We found that for a $2p$ hole, the correction to the on-site matrix element of the Hamiltonian is $\Delta H_{nn}(\mathbf{0}) = 0.85$ eV, i.e., the $2p$ valence

bands are downshifted by 0.85 eV. For the O $2s$ hole states, this correction amounts to 0.99 eV. One would expect similarly an upward shift of the conduction bands. However, the situation is somewhat different here. When an extra electron is attached to the Mg^{2+} ion, it polarizes the closed shells of the core. This is the dominant effect now because Mg^{2+} has no valence electrons. We may employ for our analysis the high-quality results obtained for a free Mg ion by Doll *et al.*[55] The correction to the ROHF Mg$^+ \rightarrow$ Mg^{2+} ionization potential was found to be 0.27 eV in Ref. 55. A similar differential correlation effect is occurring for the conduction-band states in bulk MgO. Therefore, the conduction bands are shifted downward instead of upward and a partial cancellation between *loss of ground-state correlation effects* for the valence and conduction bands is taking place. The net result is a slight increase of the gap between the valence and conduction bands, in the range of 0.5 eV. Among the different contributions discussed here, this appears to produce the smallest corrections to the gap. More advanced calculations for studying such differential correlation effects are left for future work.

To summarize the results listed in Table I, relaxation and polarization effects in bulk MgO are responsible for a reduction of the Hartree-Fock gap by 8.1 eV, which represents about 95% of the difference between the HF and experimental values, 16.2 and 7.8, respectively. Improved agreement is expected between our results and the experimental data when applying higher-quality basis sets. We mention in this context that a reduction of 3.8 eV is obtained for the HF gap when going from valence double-zeta to triple-zeta basis sets. Nevertheless, this large energy difference is mainly related to the very poor representation of the conduction-band states in the calculations with double-zeta basis functions and such effects will be less substantial by further extension of the basis sets. We also keep in mind that differential correlation effects due to the existence of a different number of electrons in the system's ground state and in the $(N\pm1)$ excited states determine a small correction in the opposite direction, i.e., a slight increase of the fundamental gap.

B. Off-diagonal matrix elements

We next discuss the effect of correlations on the widths of the different bands. For that purpose, the off-diagonal matrix elements of the effective Hamiltonian (10) have to be determined, i.e., the so-called hopping terms. At the Hartree-Fock level, these matrix elements are obtained by solving 2×2 secular equations where both wave functions are expressed in terms of localized HF orbitals [see Eqs. (4), (5), and (8)]. Relaxation and polarization effects in the nearby surroundings of the added electron (or hole) are obtained by separate SCF optimizations for the $(N\pm1)$ states. The separate optimization of the $(N\pm1)$ wave functions leads to sets of nonorthogonal orbitals. There will be thus both Hamiltonian and overlap matrix elements between the extra electron (extra hole) wave functions $\Psi_{\mathbf{0}n\sigma}^{N\pm1}$ and $\Psi_{\mathbf{R}n'\sigma}^{N\pm1}$. The calculation of such matrix elements has been recently implemented in MOLPRO.[56] It is based on the transformation of the CI vectors to biorthogonal orbitals and follows an idea suggested by

TABLE II. Nearest-neighbor (NN), $\mathbf{R}_{NN}=(1,1,0)a/2$, and next-nearest-neighbor (NNN), $\mathbf{R}_{NNN}=(1,0,0)a$, hopping matrix elements for the conduction-band Mg $3s$ and $3p$ orbitals (see text). Results of frozen-orbital CI (FO-CI) are listed in the second column; NOCI results in terms of separately optimized, relaxed orbitals (RO-NOCI) are given in the third column. All numbers are in eV.

	$t_{nn'}(\mathbf{R})$	
	FO-CI	RO-NOCI
t_{NN}		
$3s$-$3s$	0.41	0.42
$3p_{x(y)}$-$3p_{x(y)}$	0.66	0.69
$3p_{x(y)}$-$3p_{y(x)}$	0.72	0.77
$3p_z$-$3p_z$	0.13	0.13
t_{NNN}		
$3s$-$3s$	0.36	0.37
$3p_x$-$3p_x$	0.77	0.74
$3p_{y(z)}$-$3p_{y(z)}$	0.13	0.12

Malmqvist.[57] A similar approach was developed by Broer and Nieuwpoort in Groningen.[58] Instead of putting these matrix elements directly into the eigenvalue equations that determine the Bloch energies $\epsilon_n(\mathbf{k})$, we extract from these data effective hopping parameters associated with various pairs of orbitals. Comparison between such effective hopping terms and the HF off-diagonal Hamiltonian matrix elements offers an insightful picture of how correlation effects modify the intersite interactions and consequently the widths of the bands. For energetically degenerate states, the effective hopping is defined as

$$t_{nn'} = (H_{nn'} - S_{nn'}H_{nn})/(1 - S_{nn'}^2), \qquad (13)$$

where $H_{nn'}$ and $S_{nn'}$ are the Hamiltonian and overlap matrix elements between the $(N\pm1)$ states n and n'. Since the separately optimized wave functions are expressed in terms of sets of nonorthogonal orbitals, this type of secular problem is usually referred to as nonorthogonal CI (NOCI). In the case of mutually orthogonal states, $S_{nn'}$ is zero and $t_{nn'}(\mathbf{R}) = H_{nn'}(\mathbf{R})$.

Nearest-neighbor and next-nearest-neighbor (NNN) hopping matrix elements for the more diffuse conduction-band Mg $3s$ and $3p$ orbitals are listed in Table II. In the rocksalt structure, there are two O ions bridging two NN cations, whereas two NNN Mg's share a single oxygen. We designed a $[Mg_{28}O_{36}]$ cluster for calculating the NN hoppings and a $[Mg_{36}O_{47}]$ cluster for the NNN matrix elements. As active regions, we employed $[Mg_2O_6]$ and $[Mg_2O_9]$ kernels, respectively (see Figs. 5 and 6). As in the calculations for the on-site matrix elements, for each of these clusters we included in the buffer region $\mathcal{C}_B$ all metal and O ions in the first two coordination shells of the active oxygens. Since the second cluster consists of 83 atoms, we reduced the computational effort by removing the polarization functions at the
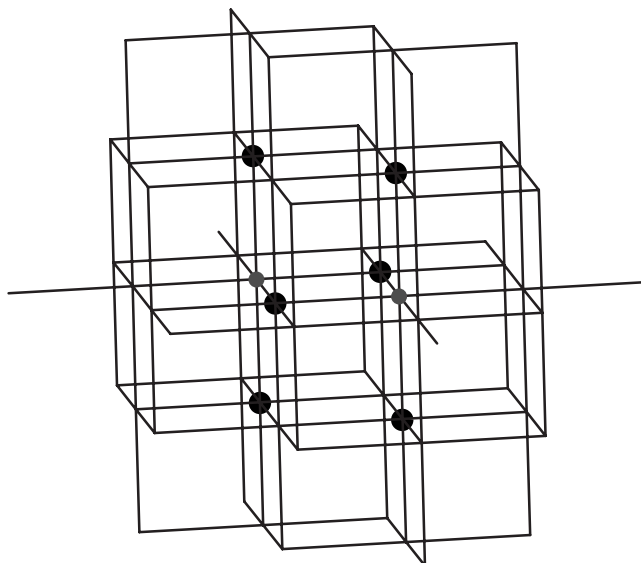

FIG. 5. Sketch of the $[Mg_{28}O_{36}]$ cluster employed for the calculation of the NN conduction-band hoppings. The active region $\mathcal{C}_A$ includes two NN Mg sites, small gray spheres, plus the bridging and apical ligands, large black spheres.

oxygen sites for this particular cluster. Two different values are given in Table II for each hopping matrix element. Results extracted from 2×2 CI calculations in terms of frozen HF Wannier orbitals are listed in the second column. In the third column, we allowed for full relaxation of the $2s$ and $2p$ orbitals of the O ions included in the active region $\mathcal{C}_A$, for each of the $(N+1)$ configuration state functions entering the 2×2 CI. As illustrated in Figs. 5 and 6, those active anions are the ligand(s) bridging two Mg sites and the ligands which are nearest oxygen neighbors of one of the active Mg sites and also of the bridging ligand(s).

The results show that the separate optimization of the $(N+1)$ wave functions induces only minor changes on the electron hoppings, in the range of a few percent. An interest-
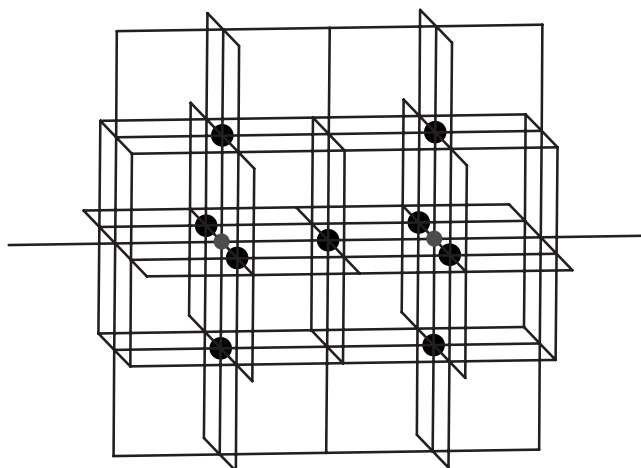

FIG. 6. Sketch of the $[Mg_{36}O_{47}]$ cluster employed for the calculation of the NNN conduction-band hoppings. The active region $\mathcal{C}_A$ includes two Mg sites, small gray spheres, and nine O neighbors, large black spheres.

TABLE III. NN, $\mathbf{R}_{NN}=(1,1,0)a/2$, and NNN, $\mathbf{R}_{NNN}=(1,0,0)a$, hopping matrix elements for the valence-band states. Results of frozen-orbital CI (FO-CI) are listed in the second column; NOCI results in terms of separately optimized, relaxed orbitals (RO-NOCI) are given in the third column. All numbers are in eV. Data for the oxygen $2s$ orbitals are also included, although the O $2s$ band is much below the O $2p$ bands. The values in parentheses include orbital relaxation effects at four additional O sites (see text).

	$t_{nn'}(\mathbf{R})$	
	FO-CI	RO-NOCI
t_{NN}		
$2s$-$2s$	0.10	0.12 (0.11)
$2p_{x(y)}$-$2p_{x(y)}$	0.32	0.37 (0.36)
$2p_{x(y)}$-$2p_{y(x)}$	0.42	0.49 (0.47)
$2p_z$-$2p_z$	0.12	0.14 (0.13)
t_{NNN}		
$2s$-$2s$	0.01	0.01
$2p_x$-$2p_x$	0.06	0.06

ing feature is that variations occur in both directions, i.e., some of the effective hoppings are slightly enlarged by taking into account short-range relaxation and polarization effects and some are reduced. Since these changes are quite small, the width (and the overall structure) of the lower conduction bands will change very little. Regarding the longer-range polarization effects, we expect that their influence on the hopping terms is negligible.

In the case of nonequivalent orbitals, neighboring Mg $3s$ and Mg $3p$, it is more difficult to define some NOCI effective hoppings and the corresponding data are not shown in Table II. Nevertheless, the effect of short-range relaxation and polarization is also small for these interactions, with changes of the CI splittings of a few meV.

The same type of analysis was applied to the $(N-1)$ O $2s^1/2p^5$ hole states. The spatial extent of the oxygen orbitals and the intersite matrix elements are significantly smaller. Since the largest relaxation effects concern orbitals at the same site (see Table I), we included in a first step only two ligands in the active regions of our clusters. Nevertheless, few other atomic shells were added around these active sites in the buffer region $\mathcal{C}_B$. We considered a $[O_{28}Mg_{10}]$ cluster for computing the relaxation effects on the NN hoppings and a $[O_{32}Mg_{11}]$ cluster for the NNN terms. The results are collected in Table III. The largest corrections arise for the NN matrix elements, with absolute values that are similar to the corrections obtained for the NN conduction-band hoppings. In relative numbers, these corrections are somewhat larger, by 10%–20% for the NN hoppings. A very different situation occurs in strongly correlated oxides such as the layered cuprates, where the existence of an antiferromagnetic spin background determines a reduction of the effective quasiparticle hoppings by a factor of 4.[59]

The trends displayed in Table III are confirmed by multireference CISD [MRCI(SD)] calculations. We correlated in these calculations the eight $2s$ and $2p$ orbitals at the two NN

oxygen sites and the reference active space included those two orbitals involved in the hopping process. The hopping matrix element is half of the energy separation between the lowest two eigenstates. The MRCI values for the $2p_x$-$2p_x$ and $2p_x$-$2p_y$ hoppings, for example, are 0.33 and 0.43 eV. These numbers are again larger than the HF results, although the magnitude of the effect is smaller as compared to the NOCI calculations. Having the data of the SCF calculations for the $(N-1)$ oxygen hole states at hand, we performed an analysis of the changes produced in the composition of the (relaxed) orbitals in the immediate vicinity of an O$^-$ $2s^1$ or $2p^5$ anion. We found that an oxygen hole is causing polarization and "bending" of the $2p$ orbitals at the NN ligand sites. The bending of the NN $2p$ orbitals toward the O$^-$ site takes place through both p-s and p_i-p_j mixing. These effects result in stronger intersite orbital overlap and explain the fact that the effective NOCI hoppings are *larger* than the corresponding HF values. A similar analysis for the conduction-band $(N+1)$ states is complicated by the presence of several sets of "active" orbitals, Mg $3s$, $3p$ and bridging O $2p$, and we could draw no clear conclusions in that case.

Extra calculations were performed for the NN hopping matrix elements with four additional oxygen sites included in the active region of the cluster, $\mathcal{C}_A$. Those are the four ligands which are nearest neighbors to both O ions involved in the hopping process. They are situated in the median plane of the segment $\mathbf{R}_{NN}=(1,1,0)a/2$. A cluster composed of 62 sites, $[O_{40}Mg_{22}]$, was employed for these calculations. The results are given in Table III in parentheses. The corrections due to relaxation and polarization at the four nearest neighbor O sites are very small, 0.01–0.02 eV. The effect of these corrections is to reduce somewhat the absolute values of the NN hoppings.

Experimental studies for characterizing the valence electronic structure of MgO have been carried out using x-ray photoelectron spectroscopy[60] and angle-resolved ultraviolet photoelectron spectroscopy.[61] The measured width of the O $2p$ bands is about 6.5 eV.[60,61] The HF valence-bandwidth is 5.50 eV and inclusion of local correlations leads to a slight broadening of the O $2p$ bands, which brings the *ab initio* result in good agreement with the experiment. For comparison, density-functional calculations within the local density approximation and using the same Gaussian basis sets as in the HF calculations predict a width of 4.68 eV for the O $2p$ bands.

The correlation induced corrections to the widths of the bands also influence the band gap. In the fcc lattice, the dispersion of the p bands at the Γ point depends on two of the nearest-neighbor hoppings, $\epsilon_x(\Gamma)=\text{const}+8t_{x,x}^{(110)}-4t_{x,x}^{(011)}+\cdots$.[62,63] With the notations from Table III, $t_{x,x}^{(011)}=t_{z,z}^{(110)}$. Corrections of 0.04 eV for $t_{x,x}^{(110)}$ and 0.01 eV for $t_{x,x}^{(011)}$ (or $t_{z,z}^{(110)}$) (see Table III) imply an upward shift of the O $2p$ bands at the Γ point and a narrowing of the fundamental gap by about 0.30 eV. For the Mg $3s$-$3p$ conduction-band complex, such changes at the Γ point are smaller because the correlation induced corrections to the $3s$-$3s$ and $3s$-$3p$ intersite matrix elements are lower.

IV. SUMMARY AND CONCLUSIONS

We have analyzed the different correlation contributions to the energy gap of MgO and to the widths of the conduc-

tion and valence bands. This was done within the quasiparticle description. As regards correlation effects, we have distinguished between relaxation and polarization around an electron or hole added to the (neutral) ground state. The net result is a reduction of the Hartree-Fock gap from 16.2 eV to a value of 8.1 eV. This has to be compared with a measured energy gap of 7.8 eV. Within the local density approximation (LDA) to density-functional theory, a gap of 5.0 eV is found. This is not surprising since LDA is known to produce too small gaps for insulators and semiconductors.

The calculations were performed with triple-zeta basis sets. Since on the Hartree-Fock level the calculated gap differs for double- and triple-zeta basis sets by 3.8 eV, one may consider the good agreement with the experimental gap as somewhat fortuitous. Triple-zeta basis sets are known, however, to produce reliable results in solids and therefore a further extension of the basis set should keep the corrections small. Presently, we are not able to work with larger basis sets.

It was shown that a large contribution to the correlation induced corrections to the fundamental gap comes from onsite and nearest-neighbor relaxation, i.e., from the immediate neighborhood of the added particle. The long-range part of the polarization generated by the extra particle also contributes substantially to the reduction of the HF gap. This long-range part can be treated in a continuum approximation, thereby using the known dielectric constant of MgO. The so-called loss of ground-state correlations makes a small contribution in MgO. The reason is that the conduction-band Wannier orbitals have predominant Mg $3s$ or $3p$ character. The added electron will essentially go thus to a Mg site where it polarizes the closed $1s^2$, $2s^2$, and $2p^6$ shells. This effect reduces the gap and counteracts the loss of ground-state correlations which occurs when an electron is removed (hole state) and therefore can no longer contribute to the correlations of the remaining ones. Finally, also changes in the widths of the bands influence the energy gap.

One surprising effect which we found is an enhancement of the width of the valence bands when local correlations are taken into account. This is the opposite one expects since correlations usually lead to band narrowing instead of broadening. It results from a slight bending of the nearest-neighbor O $2p$ orbitals toward the O$^-$ anion when we account for correlations. The bending of the nearest-neighbor ligand orbitals increases the wave function overlap and hence facilitates the hopping.

The present results prove the usefulness of band calculations based on quantum chemical techniques. They allow for well controlled approximations and a transparent interpretation of the different microscopic processes which determine the size of the energy gap and the widths of the bands.

ACKNOWLEDGMENTS

---

*Present address: Forschungszentrum Dresden-Rossendorf, Bautzner Landstrasse 128, 01328 Dresden, Germany.

[1] P. Fulde, *Electron Correlations in Molecules and Solids* (Springer-Verlag, Berlin, 1995).

[2] N. H. March, *Electron Correlation in Molecules and Condensed Phases* (Plenum, New York, 1996).

[3] P. Fulde, Adv. Phys. **51**, 909 (2002).

[4] R. McWeeny, *Methods of Molecular Quantum Mechanics* (Academic, London, 1996).

[5] T. Helgaker, P. Jørgensen, and J. Olsen, *Molecular Electronic-Structure Theory* (Wiley, Chichester, 2000).

[6] S. Suhai, Phys. Rev. B **27**, 3506 (1983).

[7] C.-M. Liegener, J. Chem. Phys. **88**, 6999 (1988).

[8] J. J. Ladik, Phys. Rep. **313**, 171 (1999).

[9] J.-Q. Sun and R. J. Bartlett, J. Chem. Phys. **104**, 8553 (1996).

[10] S. Hirata and S. Iwata, J. Chem. Phys. **109**, 4147 (1998).

[11] P. Reinhardt and J.-P. Malrieu, J. Chem. Phys. **109**, 7632 (1998).

[12] P. Y. Ayala, K. N. Kudin, and G. E. Scuseria, J. Chem. Phys. **115**, 9698 (2001).

[13] A. Abdurahman, A. Shukla, and M. Dolg, Phys. Rev. B **65**, 115106 (2002).

[14] C. Pisani, M. Busso, G. Capecchi, S. Casassa, R. Dovesi, L. Maschio, C. Zicovich-Wilson, and M. Schütz, J. Chem. Phys. **122**, 094113 (2005).

[15] S. Hirata and R. J. Bartlett, J. Chem. Phys. **112**, 7339 (2000).

[16] R. Pino and G. E. Scuseria, J. Chem. Phys. **121**, 2553 (2004).

[17] M. Albrecht and J. Igarashi, J. Phys. Soc. Jpn. **70**, 1035 (2001).

[18] M. Albrecht and P. Fulde, Phys. Status Solidi B **234**, 313 (2002).

[19] C. Buth, U. Birkenheuer, M. Albrecht, and P. Fulde, Phys. Rev. B **72**, 195107 (2005).

[20] J. Ladik and M. Seel, Phys. Rev. B **13**, 5338 (1976).

[21] J. Ladik, Phys. Rev. B **17**, 1663 (1978).

[22] W. Förner, Int. J. Quantum Chem. **43**, 221 (1992).

[23] W. Förner, R. Knab, J. Čížek, and J. Ladik, J. Chem. Phys. **106**, 10248 (1997).

[24] K. Fink and V. Staemmler, J. Chem. Phys. **103**, 2603 (1995).

[25] S. Hirata, R. Podeszwa, M. Tobita, and R. J. Bartlett, J. Chem. Phys. **120**, 2581 (2004).

[26] C. M. Zicovich-Wilson, R. Dovesi, and V. R. Saunders, J. Chem. Phys. **115**, 9708 (2001).

[27] U. Birkenheuer and D. Izotov, Phys. Rev. B **71**, 125116 (2005).

[28] A. Shukla, M. Dolg, P. Fulde, and H. Stoll, Phys. Rev. B **57**, 1471 (1998).

[29] A. Shukla, M. Dolg, P. Fulde, and H. Stoll, Phys. Rev. B **60**, 5211 (1999).

[30] A. Abdurahman, A. Shukla, and M. Dolg, J. Chem. Phys. **112**, 4801 (2000).

[31] P. Sony and A. Shukla, Phys. Rev. B **73**, 165106 (2006).

[32] J. Rubio, A. Povill, J. P. Malrieu, and P. Reinhardt, J. Chem. Phys. **107**, 10044 (1997).

[33] H. Stoll, Phys. Rev. B **46**, 6700 (1992).

[34] For a review, see B. Paulus, Phys. Rep. **428**, 1 (2006).

[35] S. Horsch, P. Horsch, and P. Fulde, Phys. Rev. B **29**, 1870 (1984).

[36] J. Gräfenstein, H. Stoll, and P. Fulde, Chem. Phys. Lett. **215**, 611

(1993).

[37] J. Gräfenstein, H. Stoll, and P. Fulde, Phys. Rev. B **55**, 13588 (1997).

[38] M. Albrecht, P. Fulde, and H. Stoll, Chem. Phys. Lett. **319**, 355 (2000).

[39] V. Bezugly and U. Birkenheuer, Chem. Phys. Lett. **399**, 57 (2004).

[40] U. Birkenheuer, P. Fulde, and H. Stoll, Theor. Chem. Acc. **116**, 398 (2006).

[41] E. Pahl and U. Birkenheuer, J. Chem. Phys. **124**, 214101 (2006).

[42] E. Pahl, U. Birkenheuer, H. Stoll, and P. Fulde (unpublished).

[43] V. R. Saunders, R. Dovesi, C. Roetti, M. Causà, N. M. Harrison *et al.*, CRYSTAL, University of Torino, Italy, 2000.

[44] U. Birkenheuer, C. Willnauer, M. von Arnim, W. Alsheimer, and D. Izotov, scientific report, Max-Planck-Institut für Physik komplexer Systeme, Dresden, 2002 (unpublished), Chap. II.1.8, p. 71 (http://www.pks.mpg.de/mpi-doc/quantumchemistry/report18.html).

[45] U. Birkenheuer (unpublished).

[46] C. Roetti, R. Dovesi, M. von Arnim, W. Alsheimer, and U. Birkenheuer, the CRYSTAL-MOLPRO interface, Max-Planck-Institut für Physik komplexer Systeme, Dresden, Germany.

[47] P. Pulay, Chem. Phys. Lett. **100**, 151 (1983); S. Saebø and P. Pulay, *ibid.* **113**, 13 (1985).

[48] H.-J. Werner, P. J. Knowles, R. Lindh, F. R. Manby, M. Schütz *et al.*, MOLPRO, Cardiff University, United Kingdom, 2006.

[49] S. S. P. Parkin, C. Kaiser, A. Panchula, P. M. Rice, B. Hughes, M. Samant, and S.-H. Yang, Nat. Mater. **3**, 862 (2004); S. Yuasa, T. Nagahama, A. Fukushima, Y. Suzuki, and K. Ando, *ibid.* **3**, 868

(2004).

[50] S. Choopun, R. D. Vispute, W. Yang, R. P. Sharma, T. Venkatesan, and H. Shen, Appl. Phys. Lett. **80**, 1529 (2002).

[51] R. C. Whited, C. J. Flaten, and W. C. Walker, Solid State Commun. **13**, 1903 (1973).

[52] S. Sasaki, K. Fujino, and Y. Takeuchi, Proc. Jpn. Acad., Ser. B: Phys. Biol. Sci. **55**, 43 (1979).

[53] M. I. McCarthy and N. M. Harrison, Phys. Rev. B **49**, 8574 (1994); R. Dovesi, C. Roetti, C. Freyria-Fava, E. Aprá, V. R. Saunders, and N. M. Harrison, Philos. Trans. R. Soc. London, Ser. A **341**, 203 (1992).

[54] J. Pipek and P. G. Mezey, J. Chem. Phys. **90**, 4916 (1989).

[55] K. Doll, M. Dolg, P. Fulde, and H. Stoll, Phys. Rev. B **52**, 4842 (1995).

[56] A. O. Mitrushchenkov and H.-J. Werner, Mol. Phys. (to be published).

[57] P.-Å. Malmqvist, Int. J. Quantum Chem. **30**, 479 (1986).

[58] R. Broer and W. C. Nieuwpoort, Chem. Phys. **54**, 291 (1981); Theor. Chim. Acta **73**, 405 (1988).

[59] L. Hozoi, S. Nishimoto, and C. de Graaf, Phys. Rev. B **75**, 174505 (2007).

[60] S. P. Kowalczyk, F. R. McFeely, L. Ley, V. T. Gritsyna, and D. A. Shirley, Solid State Commun. **23**, 161 (1977).

[61] L. H. Tjeng, A. R. Vos, and G. A. Sawatzky, Surf. Sci. **235**, 269 (1990).

[62] J. C. Slater and G. F. Koster, Phys. Rev. **94**, 1498 (1954).

[63] N. W. Ashcroft and N. D. Mermin, *Solid State Physics* (Brooks-Cole, Belmont, MA, 1976).